IEEE Open Journal of the
Industrial Electronics Society

Received 10 March 2024; revised 2 May 2024; accepted 21 June 2024. Date of publication 2 July 2024;
date of current version 8 July 2024. The review of this paper was arranged by Associate Editor D. M. D'Addona.

Digital Object Identifier 10.1109/OJIES.2024.3421649

A Novel Approach to Evaluate Robotic in Vitro Chewing Effect on Food Bolus Formation Using the GLCM Image Analysis Technique

ISURIE AKARAWITA [1] (Student Member, IEEE), BANGXIANG CHEN [1], JASPREET SINGH DHUPIA [1] (Senior Member, IEEE), MARTIN STOMMEL [2], AND WEILIANG XU [1] (Senior Member, IEEE)

[1]Department of Mechanical and Mechatronics Engineering, The University of Auckland, Auckland 1010, New Zealand
[2]Department of Electrical and Electronic Engineering, Auckland University of Technology, Auckland 1010, New Zealand

CORRESPONDING AUTHOR: ISURIE AKARAWITA (e-mail: iaka416@aucklanduni.ac.nz)

ABSTRACT In the context of food science and engineering, the in vitro chewing effect on food bolus formation is a critical area of research that explores the mechanical and textural properties of ingested materials. This article presents a pioneering approach to assess the in vitro chewing impact on food bolus formation using the gray level co-occurrence matrix (GLCM) image analysis technique. As technological advancements lead to the development of mastication robots, the need for evaluating in vitro chewed food bolus has grown. To address this challenge, a case study is conducted. The study's objectives encompass utilizing GLCM to determine the in vitro chewing cycle phase, analyzing texture features, and investigating chewing trajectory differences for beef and plant-based burger patties. Applying GLCM as a methodology, the research quantitatively analyzes textural features of food bolus formations under controlled in vitro chewing conditions. The outcomes reveal distinct differences between beef and plant-based samples through GLCM parameters. Significantly, the study identifies a consistent trend across various scenarios, indicating an increase in energy and homogeneity and a decrease in dissimilarity with an increasing number of in vitro chewing cycles. This investigation offers valuable insights into the dynamic relationship between chewing cycles and textural features in the oral processing of beef and plant-based burger patties.

INDEX TERMS Food bolus formation, image processing, in vitro chewing, mastication robots, oral processing, textural features.

I. INTRODUCTION

Chewing is a fundamental aspect of daily life, often occurring without much conscious thought. It serves not only as an essential function of food consumption and digestion but also for savoring food texture and flavor [1]. The process involves all the stimuli from vision, audio, tactile sensations, and kinesthetics collectively for the formation of the food bolus in the oral cavity. Hence, the evaluation of food bolus formation stands as a significant challenge, emphasizing its importance and complexity in the domain of scientific investigation [2], [3].

The bolus formation during mastication is usually studied by measuring the properties of the bolus and comparing them with the chewing movement, investigating both the intrinsic properties of foods and their influence on the overall chewing process [4] measured the hardness, cohesiveness, adhesiveness, and water content of steamed rice bolus at different chewing stages and found the hardness gradually decreased along the whole process, and the cohesiveness and water content of the bolus remained unchanged at first followed by a slight increase while the adhesiveness showed a rapid decrease at the beginning of chewing In another study to characterize food texture and bolus formation process, the roughness, hardness, and dryness were the dominant attributes at the start of chewing while the adhesiveness and softness were dominant at the end of chewing, and the softness and

adhesiveness were the key factors to trigger swallowing [5]. Furthermore, the chewing duration and the number of chewing cycles were found to increase with the hardness and size of the rice cracker [6]. Particle size distribution (PSD) is another important factor of the bolus that researchers often measure to understand the oral processing dynamics and evolution of the bolus [7]. In summary, the texture properties, moisture rate and PSD are typically measured to study the bolus formation process.

The rate of change in the PSD of the bolus slows down over successive chew cycles as particles larger than 2 mm are primarily chosen for chewing [7]. Furthermore, Jalabert-Malbos et al. [8] and Bleis et al. [9] stated that the particle size must be smaller than 2 mm for a food bolus to be swallowed. Jalabert-Malbos et al. [8] and Mishellany et al. [10] both highlighted that the particle size distribution of the preswallow bolus is similar and consistent across individuals when considering the same type of food. When considering meat, although natural meats do not entirely break down during mastication, there is a fiber separation process. This separated fiber is later gathered to create a lubricated bolus suitable for swallowing [11]. Moreover, in a study evaluating two types of bread boluses, in [9], the apparent viscosity has exhibited a power-law relationship, with a consistency index decreasing as chewing time progressed. Ultimately, the two bread types have reached similar values just before swallowing. Furthermore, Hosotsubo et al. [12] found that people take more time or cannot swallow if the bolus is more than 400 mm^3 in volume and more than 200 kPa in Young's modulus.

Exploring the complex relationship between food properties, particle size, and textural perspectives of chewed food boluses, numerous studies have employed different techniques, sensory analysis, rheological measurements, imaging methods, and sieving. Image analysis has served as a powerful tool in many food applications to measure particle sizes and observe the appearance features [13]. The key finding is that researchers, through the combined use of image analysis and sieving, have established a consistent correlation between the PSD of a food bolus and the hardness of the food. The AM2 Masticator has been validated by the same method using sieving and image analysis, comparing median particle sizes for both in vitro and in vivo food boluses [14]. Studies have also found the influence of one food component on the breakdown of another by using sieving and ImageJ analysis [15]. They have shown that, though diverse food combinations impact chewing patterns, the particle size at the swallowing stage is the same for peanuts in gelatine gel and peanuts in chocolate. These suggest the use of image analysis in food science related to the measurement of PSD, texture properties and moisture rate. Similarly, Bleis et al. [9] evaluated the particle size using mathematical morphology by taking monochrome images, then gray-level thresholding, hole filling, and granulometric analysis. However, sieve has failed to capture particles smaller than the finest sieve aperture, and laser diffraction has missed large particles due to technical constraints [16]. Due to this, image analysis to determine the size of food particles is seen as a fast, accurate, and dependable method, eliminating the need for tedious and time-consuming sieving and laser diffraction processes [17]. These researches emphasize the integration of image processing techniques in the analysis of food boluses, highlighting the critical role and significance of utilizing advanced visual methodologies for a more comprehensive research.

The application of image analysis has been employed to assess texture properties and moisture rate. Since spitting food out of the oral cavity interferes with natural food bolus formation [13], [18] observed the food boluses immediately before swallowing using an endoscope to evaluate their relationship with the number of chewing cycles. They have prepared 15 g of white and green colored rice for endoscopic identification. It has been suggested that grinding, mixing, and the number of chewing cycles are not crucial for cooked rice to reach the swallowing threshold, but aggregation is. This showcases how advancements in technology and research have diverted to different imaging methodologies of food bolus analysis. Volumes of apple slices have been determined by dual-view computer vision for deriving co-occurrence matrices and textural features [19]. LabVIEW processed images, extracting intensity planes, applying thresholds, and filtering for accurate identification and measurement of apple slices. A simulation model using image analysis has been successfully developed to identify the transient moisture gradient of the half-cut soybeans during the soaking and diffusion process [20]. The image processing steps have included image acquisition, segmentation, thresholding, and analysis. Similarly, Yu et al. [21] developed an automated technique to predict the moisture ratio of dried kiwi fruit slices using color and morphological feature extraction. The process has involved converting RGB to HSV and segmenting kiwifruit slice masks using color segmentation, edge detection, and contour extraction, thereby locating the pulp part and variations in pulp color. This introduces a pivotal example where an automated technique not only highlights the importance of the suggested parameters but also intricately connects to image analysis in the context of food research.

In the field of image analysis and computer vision, one widely employed technique for extracting textural information is the gray-level co-occurrence matrix (GLCM). As a powerful tool, GLCM captures the spatial relationships between pixel intensities in an image, providing a quantitative representation of texture patterns. Originally introduced by [22] in the 1970s, GLCM has since become a fundamental method in texture analysis, offering insights into the distribution of pixel pairs and their occurrence frequencies. One such research [23] has examined chewed apple boluses in vivo and in vitro by image texture analysis using GLCM. Normalized principal component analysis (PCA) has been conducted on nine parameters (energy, contrast, and correlation at 1, 10, and 30-pixel distances) to characterize apples chewed in the human mouth. However, their artificial mouth is a crunching apparatus, differing much from the oral cavity. A similar study [24] was found where GLCM and PCA were

employed to conduct image texture analysis, investigating the kinetics of bread bolus formation for four different bread types. They have used GLCM features such as angular second moment, contrast, correlation, entropy, and maximum probability and have suggested that contrast is the most effective marker for food degradation. Extracted from the normalized GLCM, Sebastian et al. [25] introduced a new feature called trace, which identifies the constant regions in an image to enhance the results. These research efforts are essential for refining methodologies and addressing challenges, ultimately paving the way for a more comprehensive understanding of the dynamic interplay between texture patterns and in vitro chewing.

In recent years, novel mastication robots have been used to simulate chewing and assess food properties, thereby increasing the demand for techniques to evaluate the chewed food bolus [14], [26], [27]. Given this consideration, the objectives of this case study are to utilize GLCM 1) to determine the in vitro chewing cycle, 2) to analyze the relationship of texture features, and 3) to analyze the relationship of chewing pattern differences, for beef and plant burger patties. GLCM has gained widespread popularity as a technique, with numerous studies successfully employing it for texture analysis across various domains. GLCM was chosen due to this reason and the demonstration of its effectiveness in various image textural analysis tasks despite the availability of alternative methods such as the local binary pattern, local binary gray level co-occurrence matrix, gray level run length matrix, and segmentation-based fractal texture analysis algorithms. In this research, GLCM is employed as a novel methodology to quantitatively analyze the textural features of food bolus formations generated under controlled in vitro chewing conditions. Hence, this approach extends the application of GLCM to analyze the properties of chewed in vitro food boluses.

II. IN VITRO CHEWING AND IMAGE ACQUISITION

In this section, the experiment protocol and the image of the food bolus were illustrated, followed by preprocessing of the images for further analysis.

A. CHEWING EXPERIMENTS

The experiments to generate food bolus were performed using a biomimetic masticating robot with a three-degree-of-freedom linkage mechanism and an artificial cavity [28]. The chewing robot was designed to simulate the molar crushing and grinding effect, generating a series of molar trajectories in the *XY* plane, as shown in Fig. 1. The molar trajectories, T1 (Trajectory) to T13, provide increasing lateral displacement during occlusion, which will result in a greater shearing effect when contacting the food. The oral cavity located at the center provides the function of containing the food and repositioning it back to the lower molar between occlusions actuated by the linear extension and contraction of pneumatic bellows. The saliva injected into the robot's oral cavity is controlled by an automatic syringe to achieve a user-specified injecting rate.

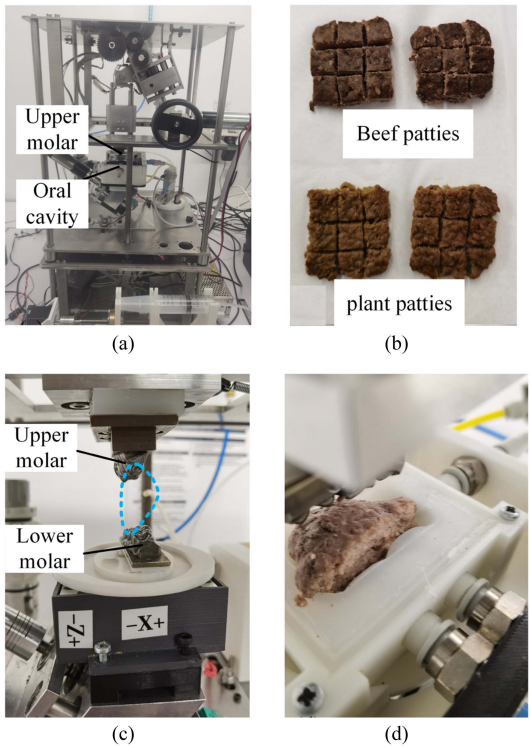

FIGURE 1. (a) Chewing robot. (b) Beef and plant based patties before chewing. (c) Trajectory 13 marked in blue dash line. (d) Food patty placed inside the artificial cavity.

TABLE 1. Chewing Tests and Their Corresponding Trajectories and Number of Cycles

Test #	Trajectories	Number of cycles
#1 & #7	#1	7
#2 & #8	#1	15
#3 & #9	#1	30
#4 & #10	#13	7
#5 & #11	#13	15
#6 & #12	#13	30

Two products were tested in this research: pure organic beef burger patties (Moreish, Palmerston North, New Zealand) and plant-based burger patties (Beyond Meat, LA, USA), obtained from local suppliers. The patties were cooked in the oven under 200 °C until the temperature in the center reached 75 °C. The cooked patties were cooled down to room temperature and then stored in the fridge at 4 °C. Prior to the test, the patties were cut into small pieces of 1 cm × 1 cm × 2 cm and weighted. One sample is fed to the robot per chewing test. The chewing parameters are present in Table 1, and each experiment setting was repeated three times. Experiment settings #1–#6 were performed with beef burgers and #7–#12 with plant-based burgers. Other than the listed parameters, cycle durations were set at 1 s and saliva flow rate at 4 ml/min (distilled water as saliva). As the chewing goes on, saliva is injected into the cavity with the specified saliva flow rate.

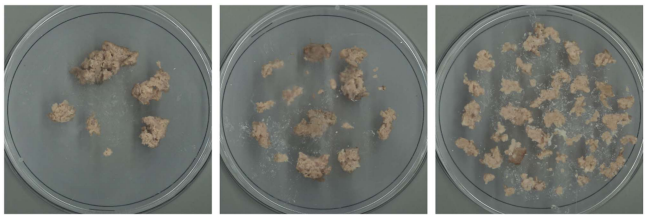

FIGURE 2. Images of BT1N7, BT1N15, and BT1N30.

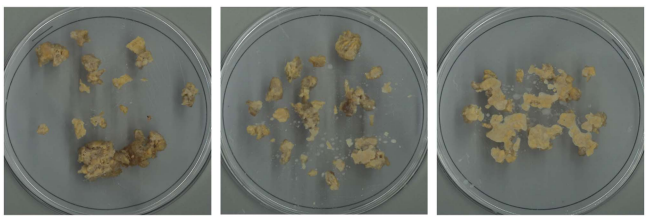

FIGURE 3. Images of PT1N7, PT1N15, and PT1N30.

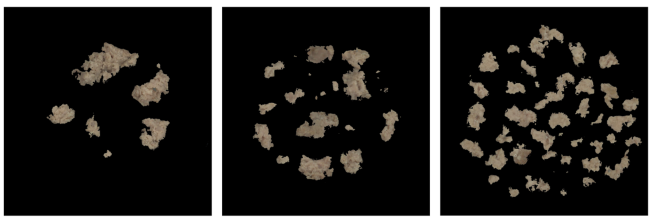

FIGURE 4. Background removed images of BT1N7, BT1N15, BT1N30.

B. IMAGE ACQUISITION AND PREPROCESSING

After the chewing, the food samples were taken out of the cavity and spread on the flat surface for scanning. For each experiment setting #1–#12, there were three repetitions, where there are 36 photos of chewed samples altogether. A standard scale with a length of 10 mm is marked on the background. The scanned images were cropped to a dimension of 1950 × 1950 pixels, as shown in Figs. 2 and 3. In these figures, the nomenclature is given as such, B = Beef, P = Plant-based, T = Trajectory, N = Number of Chewing Cycles. For example, BT1N7 means Beef, Trajectory 1, and 7 Chewing Cycles.

Then, the background removal was executed, rendering the background uniformly black, as in Fig. 4. The color thresholding method was used to remove the background. The image converted to HSV color space was used to define the range using cv2.inRange(), while a binary mask was created to set the pixels within the color range to white and the rest to black. Contours were detected within this mask using cv2.findContours() and cv2.drawContours(). Finally, the mask was applied to the original image using the cv2.bitwise_and() function to retain the pixels of the original image where the mask is white and set the rest to black, effectively removing the background. The resulting image was partitioned into 1521 tiny images, each measuring 50 × 50 pixels. This preprocessing part and all programming were executed within Visual Studio Code, using OpenCV, NumPy, Skimage, Matplotlib, os, and numpy libraries.

Then, a subsequent step involved the categorization of the 1521 tiny images into two groups. When images with a black background are used for GLCM calculations, the matrix containing pairs of black pixels can reach unacceptably high values, negatively impacting the GLCM calculations. Therefore, to maximize the number of images for analysis while minimizing the negative effects of black pixels on GLCM, the threshold of 10% was chosen. Images exceeding 10% of black pixels were excluded from the set, keeping only those tiny images associated with the food bolus and those with 10% or fewer black pixels. To this set of images, GLCM was applied to find the textural parameters.

III. PROPOSED IMAGE ANALYSIS METHODOLOGY

GLCM textural features are highly correlated with one another due to their calculation methods. Hence, a common guideline can be given for choosing, which measure to use. That is to choose one measure from each of the uncorrelated groups [29]. The group comprising dissimilarity, contrast, entropy, and variance are labeled as edge textures, having high values when visual edges are present in the neighboring pixels. Alternatively, texture features labeled as interior textures have high values for a neighborhood, which contains few coherent edges but has many subtle and irregular variations. They are homogeneity, angular second moment (ASM), correlation, GLCM mean, and possibly variance. Another categorization is done as contrast group (contrast, dissimilarity, homogeneity), orderliness group (ASM, energy, entropy), and descriptive statistics group (GLCM mean, GLCM standard deviation, GLCM correlation) [30]. Whereas another suggestion is that if only one texture measure can be used, it is recommended to choose among contrast, dissimilarity, inverse difference, moment normalized (homogeneity), or inverse difference normalized (similarity) [31]. Hence, this research considered these different categorizations when implementing GLCM textural analysis for the in vitro food boluses. The chosen textural features are energy, dissimilarity, and homogeneity, which are defined as

$$\text{ASM} = \sum_{i=0}^{\text{levels-1}} \sum_{j=0}^{\text{levels-1}} P_{ij}^2 \tag{1}$$

$$\text{Energy} = \sqrt{\text{ASM}} \tag{2}$$

$$\text{Dissimilarity} = \sum_{i=0}^{\text{levels-1}} \sum_{j=0}^{\text{levels-1}} P_{i,j}\,|i-j| \tag{3}$$

$$\text{Homogeneity} = \sum_{i=0}^{\text{levels-1}} \sum_{j=0}^{\text{levels-1}} \frac{P_{ij}}{1+(i-j)^2}. \tag{4}$$

Levels is the number of gray levels or intensity levels in the image. $P_{i,j}$ is the probability of gray level values i and j occurring in adjacent pixels in the original image within the window defining the neighborhood. i and j are the labels of the columns and rows (respectively) of the GLCM.

Then comes the problem in choosing the pixel distance and angle between the pixels for calculating energy, dissimilarity, and homogeneity. One suggestion is to calculate the GLCM parameters by considering each pixel distance and angle and taking the average [22]. The reason being that if the images are rotated, then choosing a single angle is meaningless. In this research, the images are kept without any changes to image orientation and the final bolus images are extracted in an automated process. The most used angles for GLCM calculations are 0°, 45°, 90°, and 135° [22], [31], [32], and [33]. Hence, to find the best pixel distance and the angle necessary for GLCM calculations, an analysis was conducted. For each parameter (energy, dissimilarity, and homogeneity), the difference in pixel distances was determined across various angles. That means, for each angle value and for each pixel distance, the GLCM energy was calculated for both BT1N7 and BT1N30. BT1N15 was not considered here as it is the mid chewing value. This was then plotted to visually identify the maximum difference for a particular pixel distance. If the pixel distance is one, we can see from the plot, which angle gives the maximum energy difference between BT1N7 and BT1N30. This was done separately for beef and plant, and trajectory 1 and trajectory 13 chewing cycles. The average energy difference between chewing cycles 7 and 30 of Trajectory 1 beef burger patty for pixel distances from 1 to 10 across various angles (0°, 45°, 90°, 135°) is shown in Fig. 5(a). Also, the average energy difference between chewing cycles 7 and 30 of Trajectory 13 beef burger patty, for pixel distances from 1 to 10 across various angles (0°, 45°, 90°, 135°) is shown in Fig. 5(b). This was carried out for eight such scenarios (two GLCM parameters, two types of trajectories, and two types of food).

The plot in Fig. 5(a) illustrates the difference in energy values between BT1N7 and BT1N30, facilitating a comparative analysis. The higher the difference between these, the easier it is to simplify their distinction when analyzing the GLCM textural features. The GLCM energy is calculated for each pixel pair with varying distances denoted by the *x*-axis, ranging from 1 to 10. While the plot extends up to pixel distance 10, the diminishing magnitude of energy differences indicates that further pixel distances may not offer significant insights. The plot's color signifies the angle between pixels, and the *Y*-axis depicts the energy difference magnitude. From this plot, the energy difference peaks at a pixel distance of 1 with angles 0 or 90, suggesting this is the optimal parameter for GLCM analysis to effectively distinguish between BT1N7 and BT1N30. To gain a clear understanding of plotting the curves in Fig. 5(a), the flow chart used for this algorithm is presented in Fig. 6. The same procedure was done with GLCM homogeneity to choose the optimum angle and the distance of the pixels for calculating GLCM parameters. The plot in Fig. 5(b). illustrates the difference in homogeneity values between BT1N7 and BT1N30. From the plot, the homogeneity difference peaks at a pixel distance of 1 with an angle of 90.

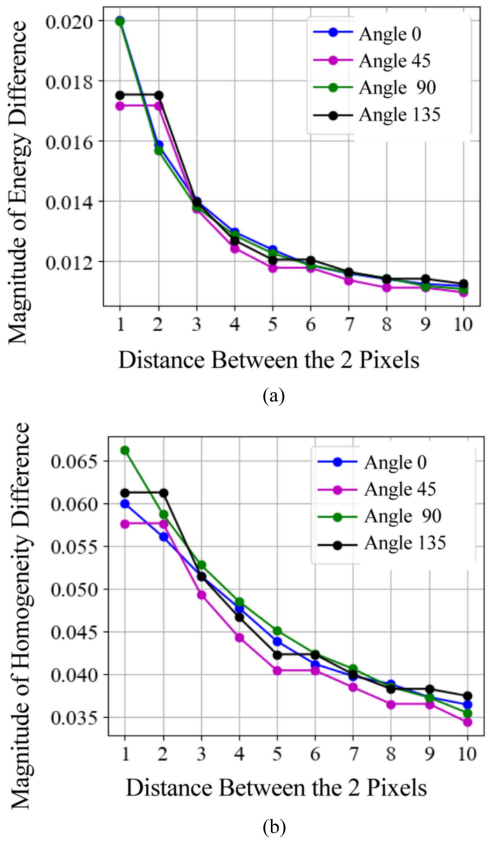

FIGURE 5. Plots illustrating the effect of pixel distance on (a) energy and (b) homogeneity difference between BT1N7 and BT1N30.

The plot in Fig. 7(a) illustrates the difference in energy values between BT13N7 and BT13N30. From this plot, the energy difference peaks at a pixel distance of 1 with an angle of 90. The plot in Fig. 7(b) illustrates the difference in homogeneity values between BT13N7 and BT13N30. From the plot, the homogeneity difference peaks at a pixel distance of 1 with an angle of 45 or 90.

In conclusion, both GLCM energy and homogeneity of BT1 suggest pixel distance 1. However, GLCM energy differences of BT1 suggest angles 0 or 90, while GLCM homogeneity differences suggest angle 90. Since an angle needs to be chosen for BT1 energy and homogeneity, angle 90 is chosen. Similarly, in conclusion, both GLCM energy and homogeneity of BT13 suggest pixel distance 1. However, GLCM energy differences of BT13 suggest angle 90, while GLCM homogeneity differences suggest angles 45 or 90. Since an angle needs to be chosen for BT13 energy and homogeneity, angle 90 is chosen. Therefore, when calculating the GLCM parameters, pixel distance 1 (d_{max}) and angle of 90 (i_{max}) are selected as they yield the maximum difference when GLCM parameters are calculated for Beef samples with trajectories 1 and 13.

The same procedure was done for trajectories 1 and 13 of the plant patty to choose the optimum angle and distance

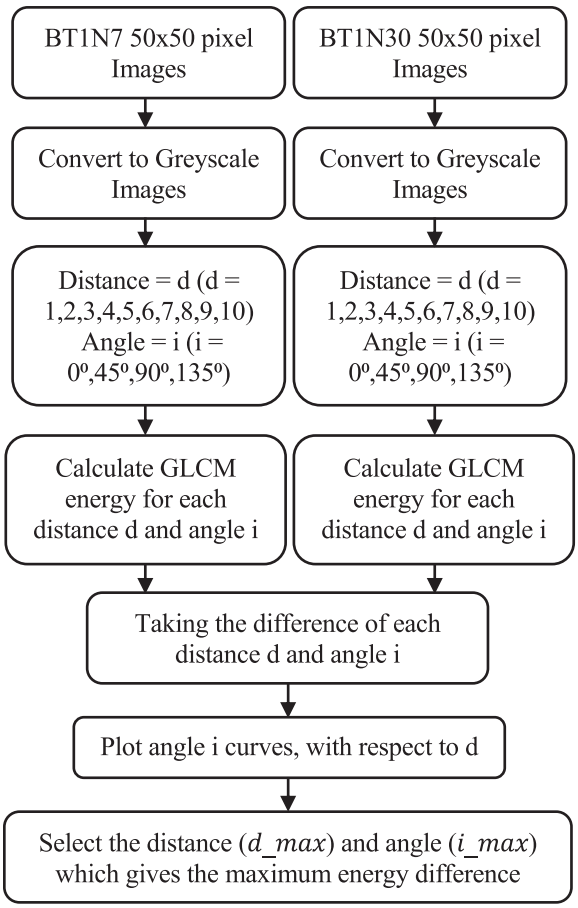

FIGURE 6. Proposed methodology for selecting the distance and angle.

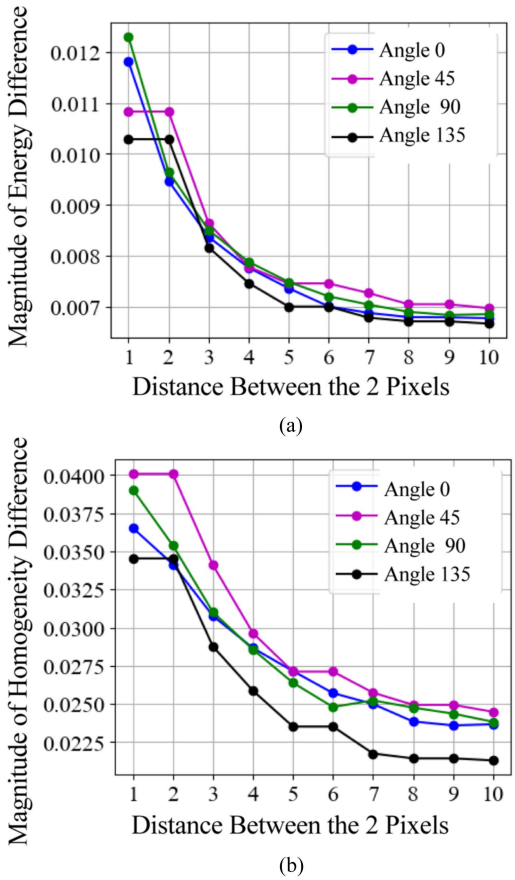

FIGURE 7. Plots illustrating the effect of pixel distance on (a) energy and (b) homogeneity difference between BT13N7 and BT13N30.

of the pixels for calculating GLCM parameters. The plot in Fig. 8(a) illustrates the difference in energy values between PT1N7 and PT1N30. From the plot, the energy difference peaks at a pixel distance of 1 with an angle of 0. The plot in Fig. 8(b) illustrates the difference in homogeneity values between PT1N7 and PT1N30. From the plot, the homogeneity difference peaks at a pixel distance of 1 or 2 with an angle of 0.

The plot in Fig. 9(a) illustrates the difference in energy values between PT13N7 and PT13N30. From the plot, the energy difference peaks at a pixel distance of 1 with an angle of 0. The plot in Fig. 9(b) illustrates the difference in homogeneity values between PT13N7 and PT13N30. From the plot, the homogeneity difference peaks at a pixel distance of 1 or 2 with an angle of 0.

In conclusion, both GLCM energy and homogeneity of PT1 suggest an angle of 0. However, GLCM energy differences of BT1 suggest pixel distance of 1, while GLCM homogeneity differences suggest pixel distance of 1 or 2. Since a pixel distance needs to be chosen for PT1 energy and homogeneity, pixel distance of 1 is chosen. Similarly, in conclusion, both GLCM energy and homogeneity of PT13 suggest angle of 0. However, GLCM energy differences of PT13 suggest pixel distance of 1, while GLCM homogeneity differences suggest pixel distance of 1 or 2. Since a pixel distance needs to be chosen for PT13 energy and homogeneity, pixel distance of 1 is chosen. Therefore, when calculating the GLCM parameters, pixel distance 1 (d_{max}) and angle of 0 (i_{max}) are selected as they yield the maximum difference when GLCM parameters are calculated for plant-based samples with trajectories 1 and 13.

In overview, the programming approach employed to attain these parameters involves utilizing feature.graycomatrix for GLCM computation, followed by the use of the skimage.feature.graycoprops function to extract the specific GLCM parameter.

IV. RESULTS

With the previously mentioned methodology, the maximum difference for GLCM energy and homogeneity of each chewing cycle is given by as follows.

1) Pixel distance 1 (d_{max}) and angle of 90 (i_{max}) for Beef samples with trajectories 1 and 13.
2) Pixel distance 1 (d_{max}) and angle of 0 (i_{max}) for Plant-based samples with trajectories 1 and 13.

Since the orientation of the images of the chewed food bolus does not change, these parameters can be derived to calculate the GLCM parameters. These results indicate that there

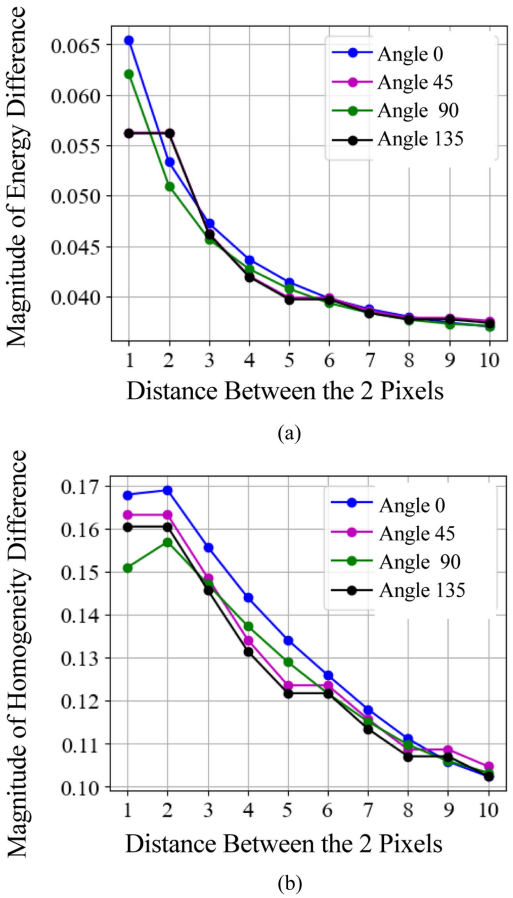

FIGURE 8. Plots illustrating the effect of pixel distance on (a) energy and (b) homogeneity difference between PT1N7 and PT1N30.

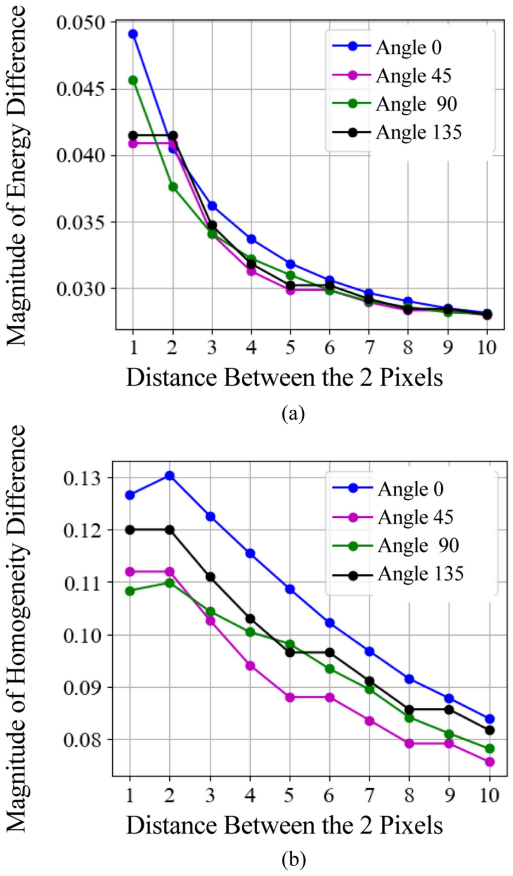

FIGURE 9. Plots illustrating the effect of pixel distance on (a) energy and (b) homogeneity difference between PT13N7 and PT13N30.

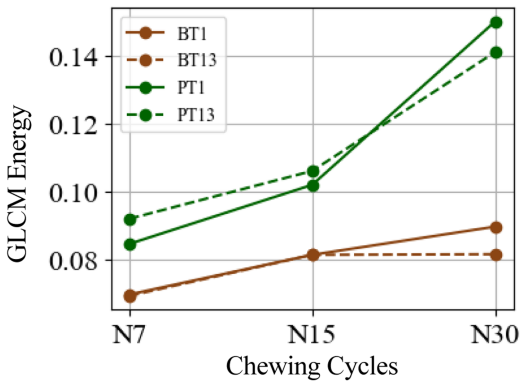

FIGURE 10. GLCM Energy of the in vitro food bolus with the number of chewing cycles.

is a distinct difference between the two food types and the difference has been identified with the use of GLCM. However, when the same methodology was applied to GLCM dissimilarity, unlike energy and homogeneity, a single maximum difference could not be found. The dissimilarity difference for N7 and N30 increased with the increase in pixel distances with each angle for all beef, plant, trajectory 1, and trajectory 13 images.

Afterwards, with the derived pixel distance and angle values, GLCM energy and homogeneity are calculated to check if there is a relationship with each chewing cycle of the food boluses. Across all scenarios involving beef and plant food boluses with trajectories 1 and 13, a consistent trend emerges. As the number of chewing cycles increases from 7, 15, and 30 (*x*-axis of the plots in Figs.), there is an increase in energy, as shown in Fig. 10, an increase in homogeneity, as shown in Fig. 11, a decrease in dissimilarity, as shown in Fig. 12. The three plots represent each type of food boluses and trajectories. This highlights the dynamic relationship between chewing cycles and textural features in the oral processing of beef and plant-based burger patties.

In this study, an analysis was conducted for the average number of bolus pieces in relation to the number of chewing cycles for both beef and plant-based boluses. The presented graph shown in Fig. 13 illustrates a comprehensive comparison of the average number of bolus pieces generated during different chewing cycles for both beef and plant-based boluses under distinct in vitro chewing trajectories. Trajectory T1, characterized by horizontal jaw movements, and T13, involving increased shear force, reveal distinctive patterns in bolus formation. Remarkably, at T1, both beef and plant boluses exhibit a consistent increase in the average number of bolus

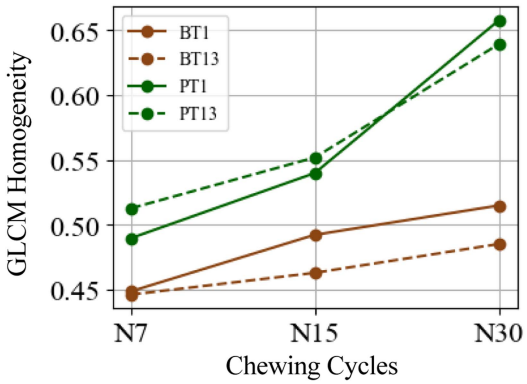

FIGURE 11. GLCM Homogeneity of the in vitro food bolus with the number of chewing cycles.

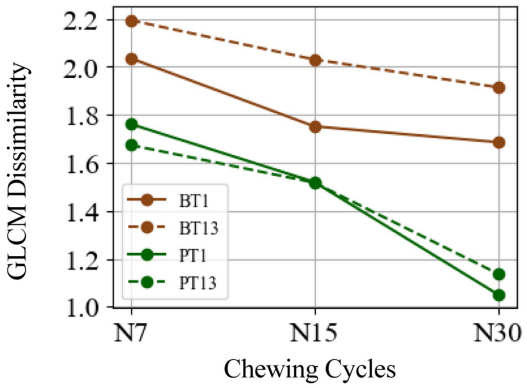

FIGURE 12. GLCM Dissimilarity of the in vitro food bolus with the number of chewing cycles.

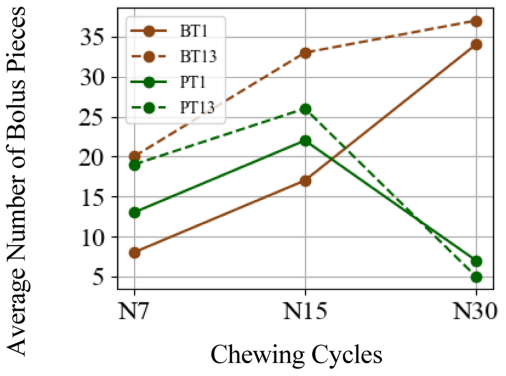

FIGURE 13. Comparison of average number of chewed bolus pieces with the number of chewing cycles.

pieces with the increase in number of chewing cycles, showcasing effective breakdown. However, under T13, interesting variations emerge. Beef boluses demonstrate a notable increase in the average number of pieces, potentially indicating enhanced fragmentation due to increased shear forces. In contrast, plant boluses under T13 exhibit a contrasting trend, with a decrease in the average number of bolus pieces, suggesting a potential shift in breakdown dynamics. The plot reveals a significant increase in the number of bolus pieces for beef burger patties as the chewing cycles increased. In contrast, plant-based burger patties demonstrate a unified chewed bolus at 30 cycles, where individual bolus pieces have combined to form more cohesive boluses. This suggests the plant-based burger patties have reached the endpoint of chewing, sooner compared to the beef burger patty. Additionally, this indicates a fiber separation process with the increase of chewing cycles in the case of beef burger patties.

V. DISCUSSION

The results highlight the effectiveness of utilizing the GLCM image analysis technique for evaluating in vitro chewing impacts on food bolus formation. GLCM parameters energy and homogeneity, revealed clear distinctions between beef and plant-based samples across different trajectories. Further analysis using derived GLCM parameters consistently demonstrated trends. Increasing chewing cycles correlated with heightened energy and homogeneity and reduced dissimilarity. This dynamic relationship between chewing cycles and textural features emphasizes the intricate oral processing of beef and plant-based burger patties. The analysis extends to examining the average number of bolus pieces concerning chewing cycles, uncovering trajectory specific patterns. Under Trajectory T1, both beef and plant boluses showed increased pieces, signifying effective breakdown. However, Trajectory T13 displayed divergent trends. Beef boluses exhibited enhanced fragmentation, while plant boluses formed a cohesive bolus, implying an earlier endpoint in chewing for the plant-based variant. These nuanced insights deepen our understanding of in vitro chewing dynamics and bolus formation, highlighting GLCM's potential in food science research.

VI. CONCLUSION

This study successfully utilized GLCM to determine the in vitro chewing cycle phase, analyze texture feature relationships, and examine in vitro chewing trajectory differences for both beef and plant burger patties. The integration of GLCM analysis in evaluating the in vitro chewing effect on food bolus formation presents a cutting-edge approach, offering researchers and food scientists a robust methodology for quantifying textural changes in a reproducible and controlled environment.

ACKNOWLEDGMENT

Author I. Akarawita would like to thank Riddet Institute, A New Zealand Center of Research Excellence (CoRE) for the Ph.D. scholarship.

REFERENCES

[1] J. Chen, "Food oral processing-A review," *Food Hydrocolloids*, vol. 23, no. 1, pp. 1–25, Jan. 2009.
[2] L. J. Pereira, M. B. Duarte Gaviao, and A. Van Der Bilt, "Influence of oral characteristics and food products on masticatory function," *Acta Odontologica Scandinavica*, vol. 64, no. 4, pp. 193–201, Aug. 2006.

[3] J. B. Hutchings and P. J. Lillford, "The perception of food texture: The philosophy of the breakdown path," *J. Texture Stud.*, vol. 19, pp. 103–115, Aug. 1988.
[4] I. Kochi et al., "Changes of bolus properties and the triggering of swallowing in healthy humans," *J. Oral Rehabil.*, vol. 48, no. 5, pp. 592–600, May 2021.
[5] D. Pu et al., "Characterization of the dynamic texture perception and the impact factors on the bolus texture changes during oral processing," *Food Chem.*, vol. 339, Mar. 2021, Art. no. 128078.
[6] E. Takei et al., "Age-related changes in functional adaptation to bolus characteristics during chewing," *Physiol. Behav.*, vol. 225, Oct. 2020, Art. no. 113102.
[7] C. S. Flynn, "The particle size distribution of solid foods after human mastication," Ph.D. dissertation, Massey Univ., Auckland, 2012.
[8] M. L. Jalabert-Malbos, A. Mishellany-Dutour, A. Woda, and M. A. Peyron, "Particle size distribution in the food bolus after mastication of natural foods," *Food Qual. Preference*, vol. 18, no. 5, pp. 803–812, Jul. 2007.
[9] F. L. Bleis, L. Chaunier, G. D. Valle, M. Panouillé, and A. L. Réguerre, "Physical assessment of bread destructuration during chewing," *Food Res. Int.*, vol. 50, no. 1, pp. 308–317, Jan. 2013.
[10] A. Mishellany, A. Woda, R. Labas, and M. A. Peyron, "The challenge of mastication: Preparing a bolus suitable for deglutition," *Dysphagia*, vol. 21, no. 2, pp. 87–94, Apr. 2006.
[11] P. Lillford, "Texture and breakdown in the mouth: An industrial research approach," *J. Texture Stud.*, vol. 49, no. 2, pp. 213–218, Apr. 2018.
[12] M. Hosotsubo, T. Magota, M. Egusa, T. Miyawaki, and T. Matsumoto, "Fabrication of artificial food bolus for evaluation of swallowing," *PLoS One*, vol. 11, no. 12, Dec. 2016, Art. no. e0168378.
[13] J. Chen, N. Khandelwal, Z. Liu, and T. Funami, "Influences of food hardness on the particle size distribution of food boluses," *Arch. Oral Biol.*, vol. 58, no. 3, pp. 293–298, Mar. 2013.
[14] A. Mishellany-Dutour et al., "Comparison of food boluses prepared in vivo and by the AM2 mastication simulator," *Food Qual. Preference*, vol. 22, no. 4, pp. 326–331, Jun. 2011.
[15] S. C. Hutchings, K. D. Foster, J. E. Bronlund, R. G. Lentle, J. R. Jones, and M. P. Morgenstern, "Particle breakdown dynamics of heterogeneous foods during mastication: Peanuts embedded inside different food matrices," *J. Food Eng.*, vol. 109, no. 4, pp. 736–744, Apr. 2012.
[16] M. A. Peyron, A. Mishellany, and A. Woda, "Particle size distribution of food boluses after mastication of six natural foods," *J. Dent. Res.*, vol. 83, no. 7, pp. 578–582, Jul. 2004.
[17] P. Morell, I. Hernando, and S. M. Fiszman, "Understanding the relevance of in-mouth food processing. A review of invitro techniques," *Trends Food Sci. Technol.*, vol. 35, no. 1. pp. 18–31, Jan. 2014.
[18] H. Fukatsu, K. Nohara, Y. Kotani, N. Tanaka, K. Matsuno, and T. Sakai, "Endoscopic evaluation of food bolus formation and its relationship with the number of chewing cycles," *J. Oral Rehabil.*, vol. 42, no. 8, pp. 580–587, Aug. 2015.
[19] D. J. Sampson, Y. K. Chang, H. P. V. Rupasinghe, and Q. U. Zaman, "A dual-view computer-vision system for volume and image texture analysis in multiple apple slices drying," *J. Food Eng.*, vol. 127, pp. 49–57, Apr. 2014.
[20] H. W. Park and W. B. Yoon, "Development of a novel image analysis technique to detect the moisture diffusion of soybeans [Glycine max (L.)] during rehydration using a mass transfer simulation model," *Food Bioprocess Technol.*, vol. 11, no. 10, pp. 1887–1894, Oct. 2018.
[21] S. Yu, H. Zheng, D. Wilson, W. Yu, and B. Young, "Vision-based moisture prediction for food drying," in *Proc. 29th Int. Conf. Mechatronics Mach. Vis. Pract.*, 2023, pp. 1–6.
[22] R. M. Haralick, K. Shanmugam, and I. Dinstein, "Textural features for image classification," *Study Media Commun.*, vol. 3, no. 6, pp. 610–621, 1973.
[23] G. Arvisenet, L. Billy, P. Poinot, E. Vigneau, D. Bertrand, and C. Prost, "Effect of apple particle state on the release of volatile compounds in a new artificial mouth device," *J. Agricultural Food Chem.*, vol. 56, no. 9, pp. 3245–3253, May 2008.
[24] C. Tournier, M. Grass, D. Zope, C. Salles, and D. Bertrand, "Characterization of bread breakdown during mastication by image texture analysis," *J. Food Eng.*, vol. 113, no. 4, pp. 615–622, Dec. 2012.
[25] B. Sebastian, A. Unnikrishnan, and K. Balakrishnan, "Grey level Co-occurrence matrices: Generalisation and some new features," *Int. J. Comput. Sci., Eng. Inf. Technol.*, vol. 2, no. 2, pp. 151–157, 2012.
[26] B. Chen, J. S. Dhupia, M. P. Morgenstern, F. Zhang, and W. Xu, "Opportunities and challenges in biomimetic robotic simulation for In vitro testing of chewable drugs," in *Proc. Int. Mech. Eng. Congr. Expo.*, 2023.
[27] S. Ren, B. Chen, X. Wang, J. Dhupia, M. Stommel, and W. Xu, "Concept of real-time prediction and evaluation system of robotic food chewing using machine vision and Deep learning," in *Proc. 29th Int. Conf. Mechatronics Mach. Vis. Pract.*, 2023, pp. 1–6.
[28] B. Chen, J. S. Dhupia, M. P. Morgenstern, J. E. Bronlund, and W. Xu, "Development of a biomimetic masticating robot for food texture analysis," *J. Mechanisms Robot.*, vol. 14, no. 2, Oct. 2021, Art. no. 021012.
[29] M. Hall-Beyer, "Practical guidelines for choosing GLCM textures to use in landscape classification tasks over a range of moderate spatial scales," *Int. J. Remote Sens.*, vol. 38, no. 5, pp. 1312–1338, Mar. 2017.
[30] M. Hall-Beyer, "GLCM texture: A tutorial," Mar. 2017. Accessed: Feb. 2024. [Online]. Available: http://lapi.fi-p.unam.mx/wp-content/uploads/Tutorial-GLCM.pdf
[31] D. A. Clausi, "An analysis of co-occurrence texture statistics as a function of grey level quantization," *Can. J. Remote Sens.*, vol. 28, no. 1, pp. 45–62, Jan. 2002.
[32] M. H. Daneshvari, E. Nourmohammadi, M. Ameri, and B. Mojaradi, "Efficient LBP-GLCM texture analysis for asphalt pavement raveling detection using eXtreme Gradient Boost," *Construction Building Mater.*, vol. 401, Oct. 2023, Art. no. 132731.
[33] D. Indra, H. M. Fadlillah, Kasman, and L. B. Ilmawan, "Rice texture analysis using GLCM features," in *Proc. Int. Conf. Elect., Comput., Energy Technol.*, 2021, pp. 1–5.

ISURIE AKARAWITA (Student Member, IEEE) received the B.S. (hons) degree in mechatronics engineering from General Sir John Kotelawala Defence University, Dehiwala-Mount Lavinia, Sri Lanka, in 2019, and the M.S. degree in industrial automation from the University of Moratuwa, Moratuwa, Sri Lanka, in 2023.

She is currently a Doctoral Research Fellow with the University of Auckland, New Zealand. Her research interests include the design and control of mechatronics systems, image processing, and the application of deep learning and machine vision.

BANGXIANG CHEN received the M.S. degree from Harbin Institute of Technology, Harbin, China, in 2016, and the Ph.D. degree from The University of Auckland, Auckland, New Zealand, in 2021, both in the mechatronics engineering.

He is currently a Postdoctoral Research Fellow with The University of Auckland, New Zealand. His research interests include mechatronics design and control of robotic systems and application of robots toward food and drug innovation.

JASPREET SINGH DHUPIA (Senior Member, IEEE) received the B.Tech. degree from the Indian Institute of Technology Delhi, New Delhi, India, in 2001, and the M.S. and Ph.D. degrees from the University of Michigan, Ann Arbor, MI, USA, in 2004 and 2007, respectively, all in mechanical engineering.

He is currently a Senior Lecturer with The University of Auckland, Auckland, New Zealand. He was an Assistant Professor with Nanyang Technological University, Singapore. His research interests include mechatronics, automation, and system identification.

Dr. Dhupia was a Technical Editor for IEEE/ASME TRANSACTIONS ON MECHATRONICS and an Associate Editor for ASME Dynamics Control and Systems Division.

MARTIN STOMMEL received the Dipl.-Ing. and Dr.-Ing. degrees in engineering from the Department of Electrical Engineering and Computer Science, University of Siegen, Siegen, Germany, in 2002 and 2010, respectively.

He was with the School of Engineering, Auckland University of Technology (AUT), Auckland, New Zealand, in 2014, where he researches machine vision, machine learning, and soft robotics, as a Senior Lecturer. He has worked on the recognition of deformable objects, classification, and 3-D vision. His methods have been applied in robotics, media and social sciences, industrial and agricultural automation, comic book analysis, and the enhancement of historic documents. Before joining AUT, he was with The University of Auckland (2013/2014), the University of Bremen (2008–2013), the University of Siegen (2002–2008), and the Silesian University of Technology (2002).

WEILIANG XU (Senior Member, IEEE) received the B.E. degree in manufacturing engineering and M.E. degree in mechanical engineering from Southeast University, Nanjing, China, in 1982 and 1985, respectively, and the Ph.D. degree in mechatronics and robotics from the Beijing University of Aeronautics and Astronautics, Beijing, China, in 1988.

He is the Chair in Mechatronics Engineering and Program Director of B.E. (hons.) in mechatronics engineering with The University of Auckland, New Zealand. Prior to Auckland, he was with Massey University, New Zealand (1999–2010), the City University of Hong Kong (1993–1998), the University of Stuttgart, Germany (1990–1992), and Southeast University, China (1988–1989).

Dr. Xu was an Associate Editors for journals: *IEEE Robotics and Automation Magazine*, IEEE TRANSACTIONS ON INDUSTRIAL ELECTRONICS, *IEEE Open Journal of Industrial Electronics Society*, *ASME Journal of Science and Engineering in Medical Diagnostics and Therapy*, and *Journal of Field Robotics*.